

FORMATION OF PLASMOID CHAINS AND FAST MAGNETIC RECONNECTION DURING NONLINEAR EVOLUTION OF THE TILT INSTABILITY

HUBERT BATY

Observatoire Astronomique de Strasbourg, Université de Strasbourg, CNRS, UMR 7550, 11 rue de l'Université, F-67000 Strasbourg, France

ABSTRACT

We investigate, by means of two-dimensional incompressible magnetohydrodynamic (MHD) numerical simulations, the fast collisional magnetic reconnection regime that is supported by the formation of plasmoid chains when the Lundquist number S exceeds a critical value (at magnetic Prandtl number, $P_m = 1$). A recently developed characteristic-Galerkin finite-element code, FINMHD, that is specifically designed for this aim in a reduced visco-resistive MHD framework, is employed. Contrary to previous studies, a different initial setup of two repelling current channels is chosen in order to form two quasi-singular current layers on an Alfvénic time scale as a consequence of the tilt instability. If $S \lesssim 5 \times 10^3$, a subsequent stationary reconnection process is obtained with a rate scaling as $S^{-1/2}$ as predicted by the classical Sweet-Parker model. Otherwise, a stochastic time-dependent reconnection regime occurs, with a fast time-averaged rate independent of S and having a normalized value of 0.014. The latter regime is triggered by the formation of two chains of plasmoids disrupting the current sheets with a sudden super-Alfvénic growth following a quiescent phase, in agreement with the general theory of the plasmoid instability proposed by Comisso et al. [*Phys. Plasmas* **23**, 100702 (2016)]. Moreover, the non-monotonic dependence of the plasmoid growth rate with S following an asymptotically decreasing logarithmic law in the infinite S -limit is confirmed. We also closely compare our results to those obtained during the development of the coalescence instability setup in order to assess the generality of the mechanism. Finally, we briefly discuss the relevance of our results to explain the flaring activity in solar corona and internal disruptions in tokamaks.

Keywords: magnetic reconnection — magnetohydrodynamics — plasmas — stars: coronae — Sun: flares

1. MOTIVATION

Magnetic reconnection is believed to be the underlying mechanism that explains explosive events observed in many magnetically dominated plasmas. This is for example the case for flares in the solar corona, or sawtooth crashes in tokamaks. It is a process of topological rearrangement of magnetic field lines that can convert a part of the magnetic energy into kinetic energy and heat (Priest & Forbes 2000). However, the timescales involved in classical two-dimensional (2D) reconnection models within the macroscopic magnetohydrodynamic (MHD) regime are too slow to match the observations or experiments. Indeed, the reconnection rate predicted by Sweet-Parker (SP) model which scales like $S^{-1/2}$ (S being the Lundquist number defined as $S = LV_A/\eta$, where L is the half-length of the current sheet, V_A is the Alfvén speed based on the magnetic field amplitude in the upstream current layer, and η is the resistivity), is too low by a few (or even many) orders of magnitude for the relevant Lundquist numbers (Sweet 1958; Parker 1957). For example, for typical parameters representative of the solar corona, S is of order 10^{12} , leading to a normalized reconnection rate of order 10^{-6} much lower than the value of $10^{-2} - 10^{-1}$ required to match the observations. Furthermore, SP theory assumes a steady-state process that cannot explain the impulsive (thus even faster) onset phase preceding the main one.

However, it has been realized in the last decade that, even in a magnetofluid approach, a new solution with a rate that is (possibly) fast enough and almost independent on S can be obtained, provided that S is higher than a critical value of order 10^4 . This new regime is supported by the formation of plasmoid chains disrupting the current

sheet in which they are born, as obtained in many numerical experiments (Samtaney et al. 2009; Bhattacharjee et al. 2009; Huang & Bhattacharjee 2010). More precisely, these plasmoids are small magnetic islands due to tearing-type resistive instabilities, constantly forming, moving, eventually coalescing, and finally being ejected through the outflow boundaries. At a given time, the system appears as an aligned layer structure of plasmoids of different sizes, and can be regarded as a statistical steady state with a time-averaged reconnection rate that is nearly (or exactly) independent of the dissipation parameters (Uzdensky et al. 2010; Loureiro et al. 2012). The linear modal theory of plasmoid instability is based on a preformed static (i.e. reconnection flows effects are neglected) unstable SP current sheet with a half-width $a \simeq LS^{-1/2}$ (Loureiro et al. 2007). Among the spectrum of many unstable modes (as $ka \leq 1$ is required if we assume a Harris-type current layer profile having an hyperbolic tangent magnetic field reversal), the linearly dominant wavenumber k_p follows $k_p L \simeq 1.4 (1 + P_m)^{-3/16} S^{3/8}$ (where $P_m = \nu/\eta$ is the magnetic Prandtl number, i.e. the ratio of viscosity coefficient ν and resistivity one η) with a corresponding maximum linear growth rate γ_p scaling as $\gamma_p \tau_A \simeq 0.62 (1 + P_m)^{-5/8} S^{1/4}$, where $\tau_A = L/V_A$ is the Alfvén time based on the current sheet half-length (Comisso & Grasso 2016; Huang et al. 2019).

Beyond these above well admitted results and despite many published papers on the subject, there is no clear consensus on a theoretical view for the plasmoids-reconnection regime including the onset phase.

The paradoxical result of infinite linear growth rate (see scaling law just above) in an ideal MHD plasma (i.e. infinite S) being incompatible with the frozen-in condition that makes reconnection impossible, an issue has been proposed by considering unstable current layers having a critical aspect ratio $L/a \simeq S^\alpha$, that is smaller than SP value in the high S limit as $0.25 < \alpha < 0.5$ (Pucci & Velli 2014). In this way, the linear growth rate becomes Alfvénic and independent of S . The value of the exponent α depends on the current profile (Pucci et al. 2018). For example, $\alpha = 1/3$ is found for the standard Harris current profile, leading to $\gamma_p \tau_A \simeq 0.62$ (using zero viscosity) with the corresponding linearly dominant wavenumber k_p following the relation $k_p L \simeq 1.4 S^{1/6}$. These results have been confirmed by numerical simulations of preformed static current layers having the correct aspect ratio value, and seem to remain true when extended to macroscopic current sheets (of fixed length) that are artificially forced to collapse asymptotically towards $a/L \sim S^{-1/3}$ and $a/L \sim S^{-1/2}$ on a time scale of order of τ_A (Tenerani et al. 2015, 2016).

On the other hand, a second theoretical issue has been proposed by Comisso et al. (2016, 2017) by investigating the plasmoid instability in a dynamically evolving (exponentially shrinking in time and reaching asymptotically a SP aspect ratio) current sheet. Without any assumption on the critical current sheet aspect ratio (for disruption onset), they employ a principle of least time to derive it as well as the corresponding dominant mode and associated growth rate. The main difference compared to the approach proposed in the first issue, is that the dominant mode is not necessarily the linearly fastest one (obtained from a static stability study), but the mode that is able to emerge first at the end of the linear phase. In this way, new scalings that are not simple S -power laws are obtained. For example, the dominant mode growth rate is predicted to follow a transition between the previous scaling as $S^{1/4}$ (for S close to S_c) and an asymptotic (for infinitely high S values) new scaling following a decreasing logarithmic dependence (see Equation 19 in Comisso et al. (2016) and Equation 32 in Comisso et al. (2017)). The growth rate can in principle easily attain super-Alfvénic values $\gamma_p \tau_A \sim 10 - 100$, while remaining finite in the infinite S limit. The precise value of the growth rate and of the corresponding wavenumber also depend on other parameters than S , that are the characteristic time scale of the current sheet formation, the thinning process, the magnetic Prandtl number, and the noise of the system.

This second issue seems to be partly supported by recent 2D numerical MHD simulations, where the coalescence instability between two parallel currents is chosen as the initial setup providing the thinning process to form the current sheet (Huang et al. 2017). Indeed, a scaling transition is effectively observed, and maximum growth rates with $\gamma_p \tau_A \simeq 10 - 20$ are obtained that are substantially smaller than values predicted by the theoretical model. The remaining differences between the simulations and the analytical model of Comisso et al. (2016, 2017) are explained by taking into account the effects of the reconnection outflow in a phenomenological model (Huang et al. 2019). Conversely, as the first theoretical model proposed by Pucci & Velli (2014) predicts constant and smaller growth rates, i.e. with $\gamma_p \tau_A \sim 1$, it consequently seems to fail to explain these numerical simulations.

Consequently, this is important to use other configurations in order to address the generality of the reconnection mechanism based on this plasmoid-unstable regime. We have thus chosen to consider a different setup, that is the tilt instability between two repelling antiparallel currents (Richard et al. 1990). Curiously, this latter configuration has been used to test ideal MHD codes (Lankalapalli et al. 2007), or more recently to study the interaction with kink instability and resulting particles acceleration (Keppens et al. 2014; Ripperda et al. 2017), but not to study magnetic reconnection associated to the plasmoids formation. Note that, a preliminary study mainly devoted to demonstrate the ability of our specifically designed MHD code, FINMHD, has been recently published (Baty 2019). In the present

work, we mainly focus on the onset phase leading to the disruption of the current sheets by the formation of many plasmoids. The ensuing statistical state with a fast reconnection rate is also addressed more superficially, as a full assessment of this state is beyond the scope of the present paper and is left to a future work. The outline of the paper is as follows. In Section 2, we present the MHD code and the initial setup for tilt instability. Section 3 is devoted to the presentation of the results. In section 4, our results are compared to those obtained using coalescence setup and to those predicted by the two theoretical models cited above. Finally, we conclude in section 5.

2. THE MHD CODE AND INITIAL SETUP

2.1. FINMHD equations

For FINMD, a set of reduced MHD equations has been chosen corresponding to a 2D incompressible model. However, instead of taking the usual formulation with vorticity and magnetic flux functions for the main variables, another choice using current-vorticity ($J - \omega$) variables is preferred because of its more symmetric formulation, facilitating the numerical matrix calculus. The latter choice also cures numerical difficulty due to the numerical treatment of a third order spatial derivative term (Philip et al. 2007). To summarize, the following set of equations is (see also Baty (2019) for more details),

$$\frac{\partial \omega}{\partial t} + (\mathbf{V} \cdot \nabla) \omega = (\mathbf{B} \cdot \nabla) J + \nu \nabla^2 \omega, \quad (1)$$

$$\frac{\partial J}{\partial t} + (\mathbf{V} \cdot \nabla) J = (\mathbf{B} \cdot \nabla) \omega + \eta \nabla^2 J + g(\phi, \psi), \quad (2)$$

$$\nabla^2 \phi = -\omega, \quad (3)$$

$$\nabla^2 \psi = -J, \quad (4)$$

with $g(\phi, \psi) = 2 \left[\frac{\partial^2 \phi}{\partial x \partial y} \left(\frac{\partial^2 \psi}{\partial x^2} - \frac{\partial^2 \psi}{\partial y^2} \right) - \frac{\partial^2 \psi}{\partial x \partial y} \left(\frac{\partial^2 \phi}{\partial x^2} - \frac{\partial^2 \phi}{\partial y^2} \right) \right]$. As usual, we have introduced the two stream functions, $\phi(x, y)$ and $\psi(x, y)$, from the fluid velocity $\mathbf{V} = \nabla \phi \wedge \mathbf{e}_z$ and magnetic field $\mathbf{B} = \nabla \psi \wedge \mathbf{e}_z$ (\mathbf{e}_z being the unit vector perpendicular to the xOy simulation plane). J and vorticity ω are the z components of the current density and vorticity vectors, as $\mathbf{J} = \nabla \wedge \mathbf{B}$ and $\boldsymbol{\omega} = \nabla \wedge \mathbf{V}$ respectively (with units using $\mu_0 = 1$). Note that we consider the resistive diffusion via the $\eta \nabla^2 J$ term (η being assumed uniform for simplicity), and also a viscous term $\nu \nabla^2 \omega$ in a similar way (with ν being the viscosity parameter also assumed uniform). The above definitions results from the choice $\psi \equiv A_z$, where A_z is the z component of the potential vector \mathbf{A} (as $\mathbf{B} = \nabla \wedge \mathbf{A}$). This choice is the one used in Ng et al. (2007) or in Baty & Nishikawa (2016), and different from the one used by Lankalapalli et al. (2007) where the choice $\psi \equiv -A_z$ is done. In the latter case, the two Poisson equations (i.e. Equations 3-4) involve an opposite sign in the right hand sides. Note that thermal pressure gradient is naturally absent from our set of equations. Note also that, an advantage of the above formulation over a standard one using the velocity and magnetic field vectors (\mathbf{V}, \mathbf{B}) as the main variables, is the divergence-free property naturally ensured for these two vectors.

2.2. FINMHD numerical method

Simulating the mechanism of magnetic reconnection in the high Lundquist number regime requires the use of particularly well adapted methods. Conventional codes generally lack some convergence properties to follow the associated complicated time dependent bursty dynamics (Keppens et al. 2013). Despite the fact that they are not commonly used, finite element techniques allows to treat the early formation of quasi-singularities (Strauss & Longcope 1998; Lankalapalli et al. 2007), and the ensuing magnetic reconnection in an efficient way (Baty 2019).

FINMHD code is based on a finite element method using triangles with quadratic basis functions on an unstructured grid. A characteristic-Galerkin scheme is chosen in order to discretize in a stable way the Lagrangian derivative $\frac{\partial}{\partial t} + (\mathbf{V} \cdot \nabla)$ appearing in the two first equations (Baty 2019). Moreover, a highly adaptive (in space and time) scheme is developed in order to follow the rapid evolution of the solution, using either a first-order time integrator (linearly unconditionally stable) or a second-order one (subject to a CFL time-step restriction). Typically, a new adapted grid can be computed at each time step, by searching the grid that renders an estimated error nearly uniform. The finite elements Freefem++ software allows to do this (Hecht 2012), by using the Hessian matrix of a given function (taken to be the current density in this study). The technique used in FINMHD has been tested on challenging tests, involving unsteady strongly anisotropic solution for the advection equation, formation of shock structures for viscous Burgers

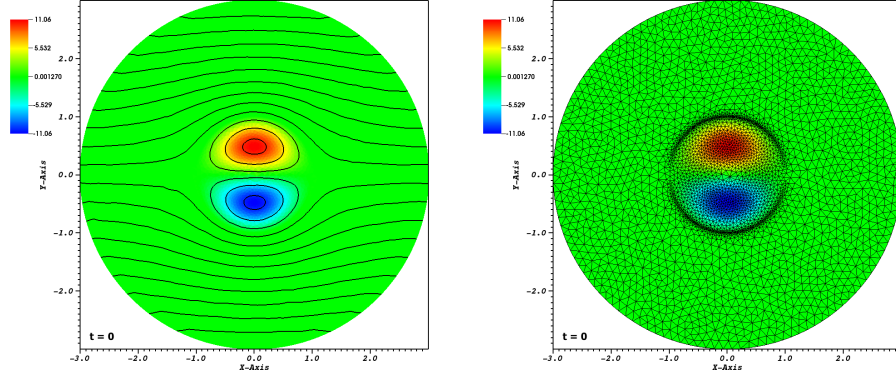


Figure 1. Initial configuration for the current density structure (colored contour map) overlaid with magnetic field lines (left panel), and overlaid with the initial grid using the density density to adapt the mesh (right panel). A moderately high value for the maximum edge size of $h_m = 0.05$ is imposed for this case using isogeometric triangles.

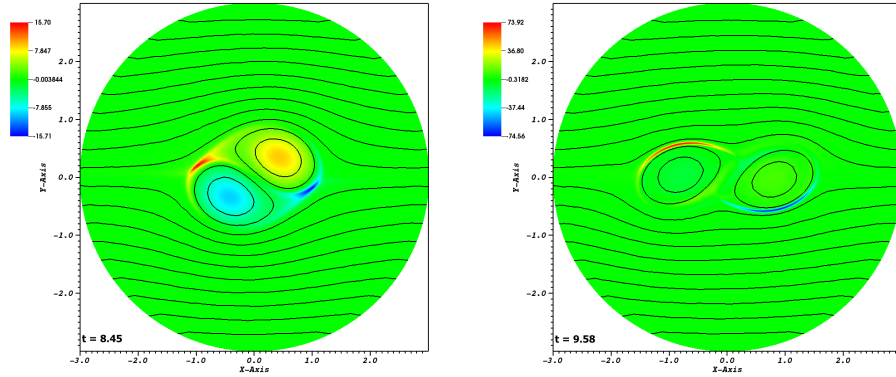


Figure 2. Same as Figure 1 for two times ($t = 8.45 t_A$ and $t = 9.58 t_A$) during the development of the tilt instability, using $S^* = 10^3$ (i.e. $\eta = \nu = 1 \times 10^{-3}$).

equation, and magnetic reconnection for the reduced set of MHD equations. The reader should refer to [Baty \(2019\)](#) for more details.

2.3. The initial setup

The initial magnetic field configuration for tilt instability is a dipole current structure similar to the dipole vortex flow pattern in fluid dynamics ([Richard et al. 1990](#)). It consists of two oppositely directed currents embedded in a constant magnetic field (see Figure 1). Contrary to the coalescence instability based on attracting parallel current structures, the two antiparallel currents in the configuration tend to repel. The initial equilibrium is thus defined by taking the following magnetic flux distribution,

$$\psi_e(x, y) = \begin{cases} \left(\frac{1}{r} - r\right) \frac{y}{r} & \text{if } r > 1, \\ -\frac{2}{\alpha J_0(\alpha)} J_1(\alpha r) \frac{y}{r} & \text{if } r \leq 1. \end{cases} \quad (5)$$

And the corresponding current density is,

$$J_e(x, y) = \begin{cases} 0 & \text{if } r > 1, \\ -\frac{2\alpha}{J_0(\alpha)} J_1(\alpha r) \frac{y}{r} & \text{if } r \leq 1, \end{cases} \quad (6)$$

where $r = \sqrt{x^2 + y^2}$, and J_0 et J_1 are Bessel functions of order 0 and 1 respectively. Note also that α is the first (non

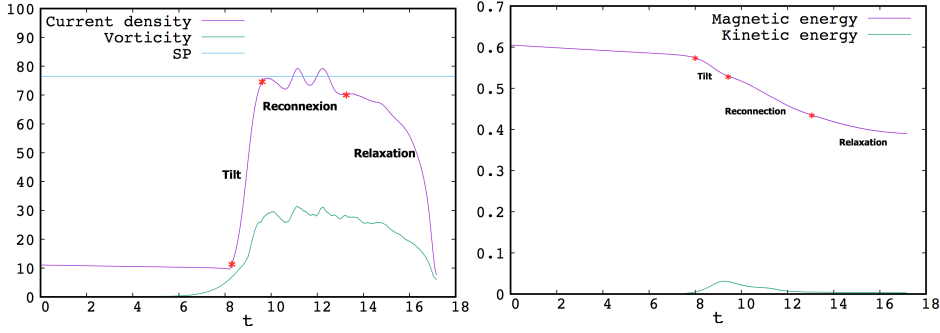


Figure 3. Time history of the maximum current density and maximum vorticity amplitudes for the run using $\eta = \nu = 1 \times 10^{-3}$ (left panel). An horizontal line indicates the average current value (i.e. 77) during reconnection phase, which also agree with the value predicted from the SP theory. Corresponding time history for the magnetic and kinetic energies in our normalized units (right panel).

zero) root of J_1 , i.e. $\alpha = 3.83170597$. This initial setup is similar to the one used in the previously cited references (Richard et al. 1990), and rotated with an angle of $\pi/2$ compared to the equilibrium chosen in the other studies (Keppens et al. 2014). Note that, the asymptotic (at large r) magnetic field strength is unity, and thus defines our normalisation. Consequently, our unit time in the following paper, will be defined as the Alfvén transit time across the unit distance (i.e. the initial characteristic length scale of the dipole structure) as $t_A = 1$. The latter time is slightly different from τ_A that is based on the half-length of the current sheet and on the upstream magnetic field magnitude. However, in our simulations we can deduce that $\tau_A \simeq t_A/2$ (see below). In usual MHD framework using the flow velocity and magnetic variables, force-free equilibria using an additional vertical (perpendicular to the $x - y$ plane) can be considered (Richard et al. 1990), or non force-free equilibria can be also ensured through a thermal pressure gradient balancing the Lorentz force (Keppens et al. 2014). In our incompressible reduced MHD model, as thermal pressure is naturally absent, we are not concerned by such choice.

In previous studies using a similar physical setup, a square domain $[-R : R]^2$ was taken with R large enough in order to have a weak effect on the central dynamics. For example a standard value of $R = 3$ is taken in Baty (2019). In the present work, a choice of using a circular domain with a radius $R = 3$ is done. We have checked that it does not influence the results compared to the square domain setup. However, this allows the use of a lower number of finite-element triangles (as the circle area is evidently smaller than the square for the same radius value R), and this also simplifies the numerical boundary treatment as only one boundary instead of four in our finite-element discretization are needed.

A stability analysis in the reduced MHD approximation using the energy principle has given that the linear eigenfunction of the tilt mode is a combination of rotation and outward displacement (Richard et al. 1990). Instead of imposing such function in order to perturb the initial setup, we have chosen to let the instability develops from the initial numerical noise. Consequently, an initial zero stream function is assumed $\phi_e(x, y) = 0$, with zero initial vorticity $\omega_e(x, y) = 0$. The values of our four different variables are also imposed to be constant in time and equal to their initial values at the boundary $r = R$.

3. RESULTS

3.1. Initial development of the tilt instability and SP reconnection regime

The initial current structure with a few magnetic field lines are reported in Figure 1 (left panel), with the initial mesh that is adapted using the Hessian matrix of the current density distribution (right panel). This arbitrary choice of current density is justified by the fact that, first the initial dynamics of the tilt instability is driven by the current distribution (i.e. this is an ideal current driven MHD instability), and second the ensuing magnetic process is controlled by the structure of the current layers. Numerical parameters defining the maximum edge size (h_m) and the anisotropy of the triangular mesh have been also adapted from case to case. Indeed, the value of h_m must be decreased as small resistivity/viscosity coefficients are employed in order to capture the small scale turbulence, leading however to a higher number of triangles and increase of time computing. The efficiency of the latter procedure is demonstrated in Baty (2019).

First, we focus on moderately low values of the resistivity and viscosity, and for simplicity we also assume a fixed Prandtl number, $P_r = \nu/\eta = 1$ in the whole paper. The early time evolution of the system corresponding to the tilt

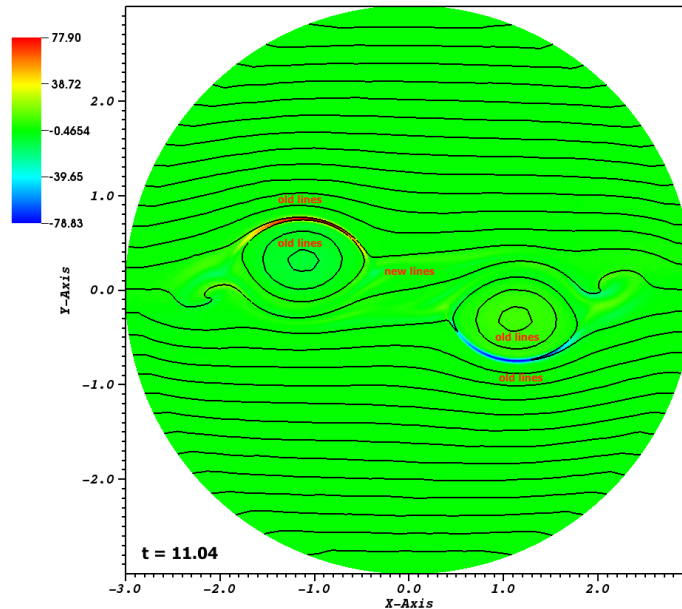


Figure 4. Same as Figures 1-2 for a later time ($t = 11.04 t_A$) showing the reconnection process with a few magnetic field lines.

instability is well documented (see the previously cited studies). It corresponds to the linear stability analysis, where the pair of oppositely directed currents tend to repel one another giving rise to a rotation. This is illustrated in Figure 2 at two times during the instability development, for a case employing an inverse resistivity value $S^* = 1/\eta = 10^3$. Note that, the sense of rotation (clockwise in Figure 2) is not predetermined and depends only on the numerical noise. This rotation causes two new regions of enhanced current density (having opposite sign) at the leading edges of the vortices because of an associated outward component of the linear displacement, taking the form of two bananas. These two regions are the relevant forming current layers of our study.

The time history of the maximum current density and vorticity amplitudes (taken over the whole domain) are shown to increase exponentially in time, and to rapidly dominate the equilibrium values (approximately 10 for the current density at $t \simeq 8 t_A$), as illustrated in Figure 3 (left panel). Note that, there is a small time delay between the current and vorticity increase. We have checked that, the associated linear dynamics follow the expected exponential time increase like $e^{2.6t}$ and $e^{1.4t}$ for the current density and vorticity respectively in agreement with stability theory (see [Baty \(2019\)](#) and references therein). During the linear and ensuing nonlinear phases of the tilt development, the kinetic energy (see right panel of Figure 3) increases in correspondence with a small decrease of the magnetic energy (the sum of both being conserved before reconnection takes place). The reconnection is triggered just before the saturation observed in current density (second asterisk in Figure 3). Subsequently, a steady-state reconnection regime is obtained with nearly constant current density/vorticity structures. The oscillations (in the maximum current density and vorticity) around average values are due to the sloshing phenomenon, as described in the coalescence problem between two magnetic islands ([Knoll & Chacón 2006](#)), because of the magnetic pressure buildup effect in thin current sheets. An average value of 77 is evaluated for the maximum current density during magnetic reconnection, in agreement with SP theory (see below). The process of magnetic reconnection between each current channel (circular magnetic field lines) and the background magnetic field (open straight field lines) is clearly visible in Figure 4, where the new reconnected field lines are also plotted. Finally, a last phase that is a relaxation towards a new state free of closed circular magnetic field lines is obtained. The latter phase is shown to begin (spotted by the last asterisk in Figure 3) when roughly 80 – 90 per-cent of the free magnetic energy is released. The detailed structure of the current sheets structure, the adapted mesh, and corresponding magnetic field lines during reconnection are shown in Figure 5. Indeed, one can clearly see in right panel of Figure 5, the few tens of elements covering the width of the current layer, thus illustrating the efficiency of our dynamically adapting mesh procedure.

In order to evaluate the local Lundquist number at saturation, $S = LV_A/\eta$, where L is the half-length of each current layer and V_A is the Alfvén velocity based on the upstream magnetic field magnitude B_u measured front of the layer,

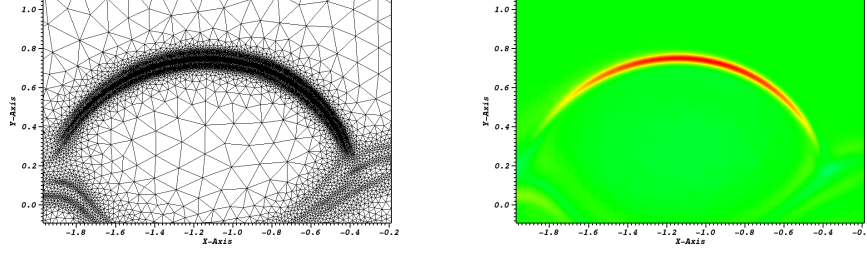


Figure 5. Zoom-in of one current sheet taken from previous figure (left panel), and corresponding adapted mesh (right panel).

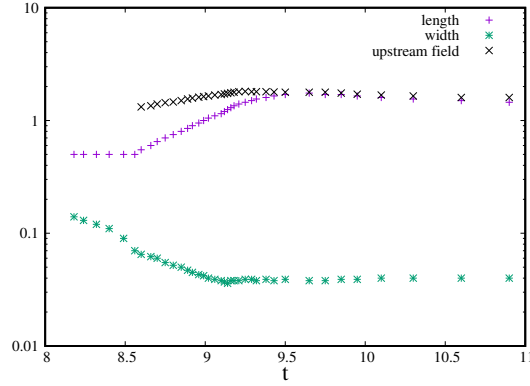


Figure 6. Time history of the characteristics of the forming current sheet (length $2L$, width $2a$, and upstream magnetic field amplitude B_u) for the run using $\eta = \nu = 1 \times 10^{-3}$ (i.e. $S^* = 10^3$).

we have followed the time history of the length ($2L$), the width ($2a$), and the upstream magnetic field amplitude (B_u). More precisely, the length and width are deduced by evaluating the locations where the current density is decreased by a factor of two compared to the maximum current density (i.e. obtained at the centre of the current layer). The value of B_u (see Figure 8) is the magnetic field measured in the current region with closed circular field lines, and it is slightly larger than the value measured in the region opposite to the current sheet with open nearly straight field lines because of the asymmetry. The results that are plotted in Figure 6 for $S^* = 10^3$, show that the three parameters are varying in time during the current sheet formation, and not only the width as assumed for example in theoretical models (Comisso et al. 2016, 2017). Second, a value of $S = 1500$ is deduced during reconnection phase, as $B_u \simeq 1.8$ and $L \simeq 0.85$ for this run.

Finally, we have compared the time evolution of the system in four different runs using inverse resistivity values $S^* = 500, 666, 1000$, and 1428 . The results obtained for the maximum current density and vorticity are plotted in Figure 7. The respective corresponding S values have been estimated to be $S = 625, 890, 1500$, and 2100 , and remain substantially lower than the critical value $S_c \simeq 10^4$ required for plasmoid formation. Note that The values of L and V_A used to deduce the above S values, slightly increase when the resistivity is decreased for $\eta \gtrsim 0.0005$, and they become approximately constant for smaller resistivity values. The characteristic reconnection time τ_r can be determined in different equivalent ways. The simplest one is to take the whole duration of the process, and it corresponds to the elapsed time between the saturation (first peak) and the final time when the current density in Figure 3 returns to a very small value corresponding to a new state (free of closed magnetic field lines). A second way is to measure the level of maximum current amplitude J_{max} during reconnection (horizontal line in Figure 3), and to multiply it by the resistivity, as ηJ_{max} is a measure of the reconnection rate (inverse of τ_r) for a steady-state process. We have checked that the reconnection rate for $S \lesssim 10^4$ closely follows a SP scaling, as $J_{max} \simeq 2 \times S^{1/2}$ (see also Figure 14), in close agreement with theoretical prediction of $J_{max} = B_u/a \simeq B_u S^{1/2} (1 + P_r)^{-1/4} / L$ as the SP aspect ratio itself is predicted to be $L/a \simeq S^{1/2} (1 + P_r)^{-1/4}$ (Comisso & Grasso 2016; Park et al. 1984). In a similar way, the maximum

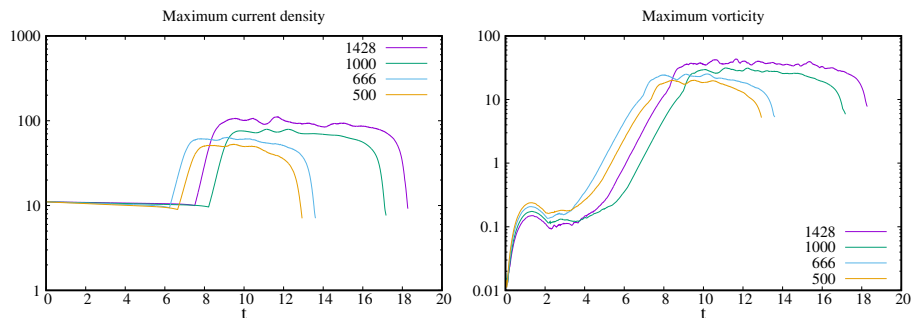


Figure 7. Time history of the maximum current density (left panel), and maximum vorticity (right panel) amplitudes for 4 runs employing inverse resistivity values S^* (between 500 and 1428).

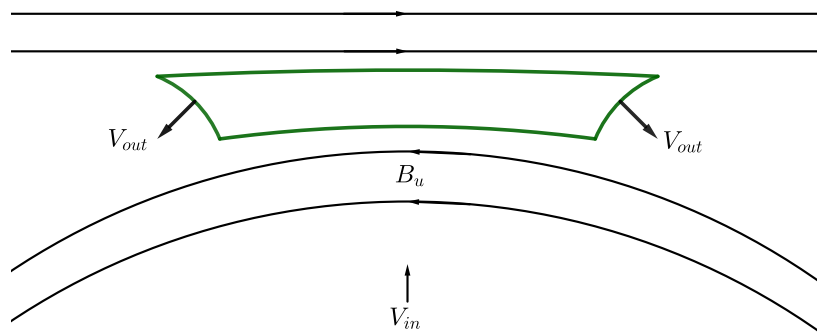


Figure 8. Schematic diagram showing the simplified geometry of magnetic field lines and of one of the two associated SP-like current sheets formed by the tilt instability.

vorticity is shown to follow a SP scaling, as $\Omega_{max} \simeq 0.75 \times S^{1/2}$, that is a factor of two smaller than predicted by the theoretical formula $\Omega_{max} = V_o/a \simeq S^{1/2}(1 + P_r)^{-3/4}V_A/L \simeq 1.4 \times S^{1/2}$ (V_{out} being the outflow SP velocity, $V_{out} \simeq (1 + P_m)^{-1/2}V_A$). This factor of two clearly comes from the asymmetric geometry of the current sheet, as schematized in Figure 8. $\Omega_{max} = V_{out}/(2a)$ is consequently a better definition formula for our problem.

3.2. Formation of a few plasmoids close to the critical Lundquist number S_c

Exploring now lower resistivity values, situated in a range $[5 \times 10^{-4} : 2.5 \times 10^{-4}]$, corresponding thus to S^* in the range $[2 \times 10^3 : 4 \times 10^3]$, lead to estimated S values in a range $[3100 : 6700]$ close to S_c from our simulations. The time history of the maximum current density is plotted in right panel of Figure 9 for 3 different S^* values. First, we note that the formation of plasmoids occurs sooner when S is higher. For example, for $S^* = 2857$, a first single plasmoid is seen to form close to the first peak ($t \simeq 8.5 t_A$). However, they can appear earlier for $S^* = 4000$ or equivalently $S = 6700$ (i.e. before the first current peak) with two plasmoids invading each current sheet at $t \simeq 9.5 t_A$. For, the highest resistivity case (i.e. for $S^* = 2000$), a single plasmoid is seen to form very lately (i.e. at $t \simeq 11.5 t_A$) on one current sheet, as also seen in the corresponding left panel of Figure 9. The ability of our code to capture the plasmoid structure is illustrated in Figure 10, showing a zoom on current density with the associated adapted grid. Note that, for the run employing $S^* = 2000$, the tilt instability has led to a sense of rotation of the initial setup in the opposite sense (i.e. counter clockwise) compared to the run of Figure 2.

Thus we consider that the critical Lundquist number is $S_c \simeq 5 \times 10^3$ for our tilt setup. This is a factor of two smaller than the currently admitted value of 10^4 . However, this is also significantly lower than the critical Lundquist deduced from MHD simulations using the coalescence setup where $S_c \simeq 3 \times 10^4$ is reported (Huang & Bhattacharjee

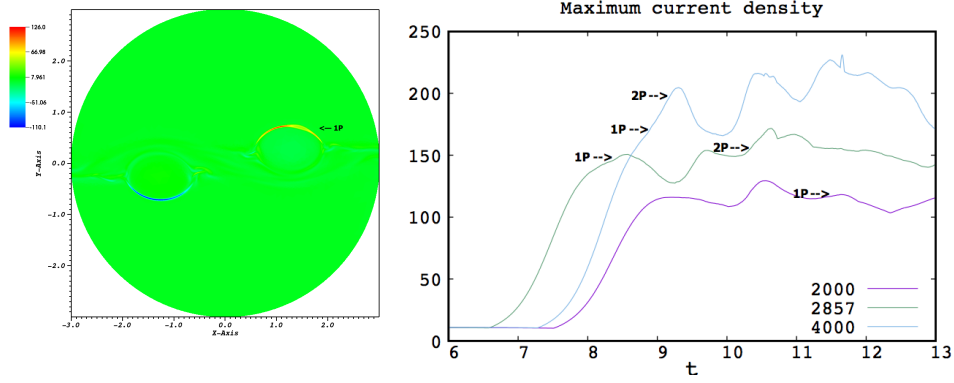


Figure 9. (Left panel) Colored contour map of the current density during reconnection phase at $t = 11.5 t_A$, for an run employing an inverse resistivity value $S^* = 2000$. A single plasmoid (label $1P$) is formed on the right current sheet. (Right panel) Time history of the maximum current density for 3 runs (employing $S^* = 2000, 2857, 4000$). The label $1P$ indicates the early formation of a single plasmoid on one current sheet and $2P$ the presence of two plasmoids on the same sheet.

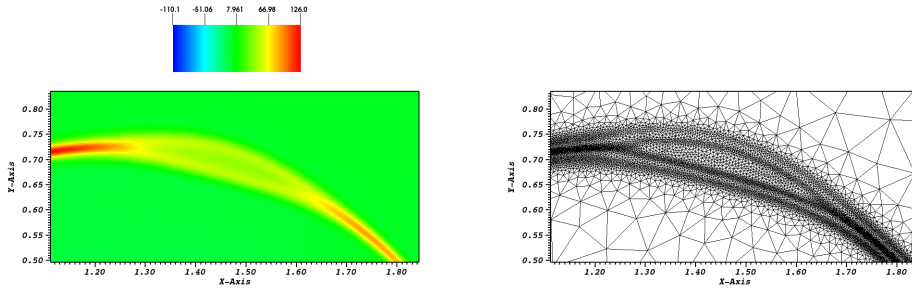


Figure 10. Zoom-in of the current density taken from the previous figure (left panel), and corresponding adapted mesh (right panel).

2010; Huang et al. 2017).

3.3. Formation of many plasmoids in the high Lundquist regime and associated fast reconnection

We focus on runs using higher Lundquist values, with S^* in a range $[6 \times 10^3 : 5 \times 10^5]$, translating into S values in the approximated range $[1 \times 10^4 : 1 \times 10^6]$. The results of time evolution of the maximum current density for a few runs in this S range are reported in Figure 11. As illustrated on the curve (case for $S^* = 2.5 \times 10^4$), 3 asterisks are used to indicate, the beginning of the tilt phase, the early formation of plasmoids, and the disruption of the current layers by the plasmoids successively. At time spotted by the second asterisk, the plasmoids are barely visible as their amplitude remain smaller than the (forming) current sheet contribution. Note that the second asterisk also coincides with an abrupt change of slope in the current density. At time spotted by the third asterisk, the plasmoids are able to fully disrupt the current layers that consequently lose their integrity, as shown in Figure 12 for two runs. Note that a contour map using a saturated value significantly lower than the maximum current density is necessary to distinguish the plasmoids at disruption time. The disruption is subsequently followed by a stochastic reconnection phase with time oscillations of the maximum current density around an average value. We have observed that the number of plasmoids is maximum at disruption and fluctuates during magnetic reconnection process, as new plasmoids are constantly forming, moving, eventually coalescing (giving thus monster plasmoids), and finally being ejected through the two end layers. The transition between a current layer slightly modified by the early growth of the plasmoids (upper panel) and a fully disrupted layer (lower panel) is illustrated in Figure 13 for the run with $S = 3.5 \times 10^5$. The formation of secondary current sheets giving rise to secondary plasmoids, and the coalescence effect between primary plasmoids leading to bigger plasmoids, are observed only at a time following the disruption (i.e. at time spotted by the third

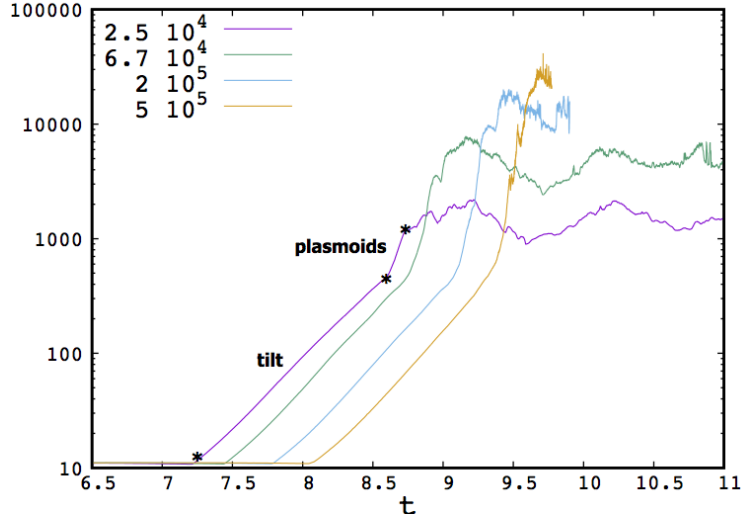


Figure 11. Time history of the maximum current density for different runs employing inverse resistivity values S^* in the range between 2.5×10^4 and 5×10^5 . Note that for the two highest cases, only the early reconnection phase is simulated. For the case employing the lowest S^* , Three asterisks are added indicating, the beginning of the tilt evolution, the early formation of the first plasmoids, and the obtention of the stochastic reconnection regime (time at which a maximum number of plasmoids is observed) successively.

asterisk). This gives support to our assumption (see below) that the phase between the second and third asterisk corresponds to a linear one for the plasmoids growth. At a given time during reconnection, the system thus appears as two aligned layer structures with a relatively high number of plasmoids (10 for $S^* = 2.5 \times 10^4$, and 20 for $S^* = 2 \times 10^5$ runs) of different sizes.

We can define two parameters characterizing the plasmoids development. The first one is the time needed for the first plasmoids to appear once the current sheet begins to form, i.e. the time delay between the first two asterisks in Figure 11, which we call t_p . The second one is deduced from the slope in current density observed between the second and third asterisk that can be fitted as $e^{\gamma_p t}$. γ_p can thus be interpreted as an instantaneous maximum growth rate. We have reported in Figure 14 (left panel), the values estimated from our runs of the two previously defined parameters (t_p and γ_p) as functions of S .

First, one can observe that the characteristic time t_p rapidly converges towards a value of $1.2 t_A \simeq 2.4 \tau_A$ that becomes rapidly independent of S . A more complex non monotonic dependence is obtained for the maximum growth rate. Indeed, γ_p is shown to follow a fitted scaling law $\gamma_p t_A = 0.9 S^{1/4} \simeq S^{1/4}$ only for a limited range of S values between 6×10^4 and 2×10^5 . Indeed, this agrees with the theoretical SP stability predicting $\gamma_p L/v_A = 0.62 S^{1/4}(1 + P_m)^{-5/8}$ (Comisso & Grasso 2016). For lower S values, our γ_p values are significantly lower than expected values from SP stability theory. For the highest S values, a transition towards a dependence scaling as $K \ln(CS^{-1/3})$ in agreement with the asymptotic solution of Comisso et al. (2016) (K and C being constants, see Equation 19 in their paper). The value of K is arbitrarily adjusted to unity, as it depends on different factors of order unity. This is not the case for the value of C that is adjusted to the very high value of 10^{10} , as it is mainly determined by a small parameter ω_0 representing the unknown noise. Thus, we can infer a noise level of order 10^{-10} in our simulations, as $C \sim 1/\omega_0$. The maximum value obtained for γ_p is $\gamma_p t_A \simeq 20$, leading thus to $\gamma_p \tau_A \simeq 10$.

An additional parameter characterizing the plasmoids development is the maximum number of plasmoids n_p (at a time close to third asterisk in Figure 11). The results obtained for the different runs (right panel of Figure 14), show again a convergence for intermediate S values towards a scaling law, that is $n_p \simeq 0.2 \times S^{3/8}$, in close agreement with the maximum wavenumber predicted from SP stability theory as $k_p L = 1.4 \times S^{3/8}(1 + P_m)^{-3/16}$, using also $n_p = Lk_p/(2\pi)$. Again, for highest S values, a transition to another dependence in agreement with the asymptotic solution of Comisso et al. (2016) is observed (see equation (18) where $k_p \propto S^{1/6}[\ln(CS^{-1/3})]^{5/6}$). The highest value for the number of observed plasmoids is $n_p \simeq 22$ for $S \simeq 10^6$.

Finally, we have plotted in Figure 15 (left panel) the maximum current density obtained at saturation as a function of S for all the runs. The results clearly show a transition between two regimes at a critical Lundquist $S_c \simeq 5 \times 10^3$. Indeed, the values for lower S values perfectly follow a Sweet-Parker scaling as $2 \times S^{1/2}$, while another scaling increasing linearly with S is obtained for higher S values as $0.033 \times S$. A similar results ensues for the maximum vorticity (right panel in Figure 15), where a transition between a SP scaling as $0.75 \times S^{1/2}$ and a linear one scaling as $0.0125 \times S$ occurs.

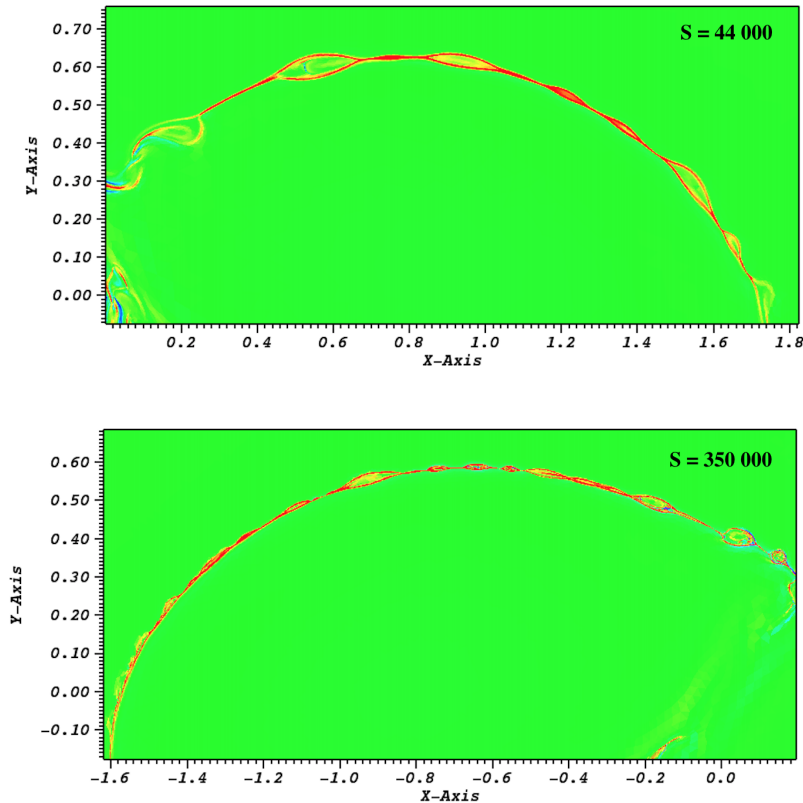


Figure 12. Zoom-in of one current sheet (colored contour map of current density with a scale saturated to 300) obtained at an early time during the reconnection phase (i.e. at a time close to the third asterisk in previous figure) for two runs employing inverse resistivity values $S^* = 2.5 \times 10^4$ (upper panel), and $S^* = 2 \times 10^5$ (lower panel). The corresponding evaluated S numbers are indicated on the plots.

As concerns the reconnection rate, constant values of $\eta J_{max} \simeq 0.05$ (independent of S) is deduced in the plasmoid regime corresponding to a normalized rate (by dividing by $V_A B_u$) of 0.014. This value is in very good agreement with the value expected from previous studies, and also from the theoretical estimate of $\epsilon_c(1 + P_m)^{-1/2} \simeq 0.012$, where $\epsilon_c \simeq 1.7 \times 10^{-2}$ is deduced from the expression $S_c = \epsilon_c^{-2}(1 + P_m)^{1/2}$ (Comisso & Grasso 2016).

4. COMPARISON WITH THEORY AND PREVIOUS STUDIES

First, from our knowledge, this study is the first one to address into detail the reconnection process associated with the nonlinear evolution of the tilt instability. Interesting results, even in the SP regime are obtained. Indeed, two forming twin current sheets (with current density of opposite sign) drive a steady-state reconnection in agreement with classical scaling laws given by the famous Sweet-Parker model. A slight amendment (by a factor of two) for the vorticity of the outflow is however required due to the particular asymmetry associated with the curved geometry of the current layers (see Figure 8).

In our study using the tilt instability as a triggering mechanism to form the current sheets, the transition from a SP reconnection process to a plasmoid-dominated regime occurs for a critical Lundquist number $S_c \simeq 5 \times 10^3$. This is a factor of two lower than the often-quoted $S_c \sim 10^4$ value in the literature. However, there is no precise universal value, as it depends on different parameters like, the current sheet geometry (via the choice for the initial setup), the magnetic Prandtl number, and also the noise amplitude (via the numerical scheme in our study). The exact definition of the Lundquist number can also differ slightly from one study to another. In the case of the numerical study using the coalescence instability, a value of $S_c \sim 3 \times 10^4$ has been reported in simulations assuming zero explicit viscosity. Even for Lundquist number very slightly lower than S_c , the formation of a transient single plasmoid is observed to occur at a relatively late time, with no real impact on the SP reconnection rate (see Figures 9-10).

Focusing on the plasmoid-dominated regime, we have examined the growth of the plasmoids, from their birth to their ensuing disrupting effect on the current sheets. An important reference time scale for comparing the latter growth is the time scale for forming the current layers, that is given by $\tau = 0.38 t_A \simeq 1 \tau_A$, as the tilt mode is an ideal MHD

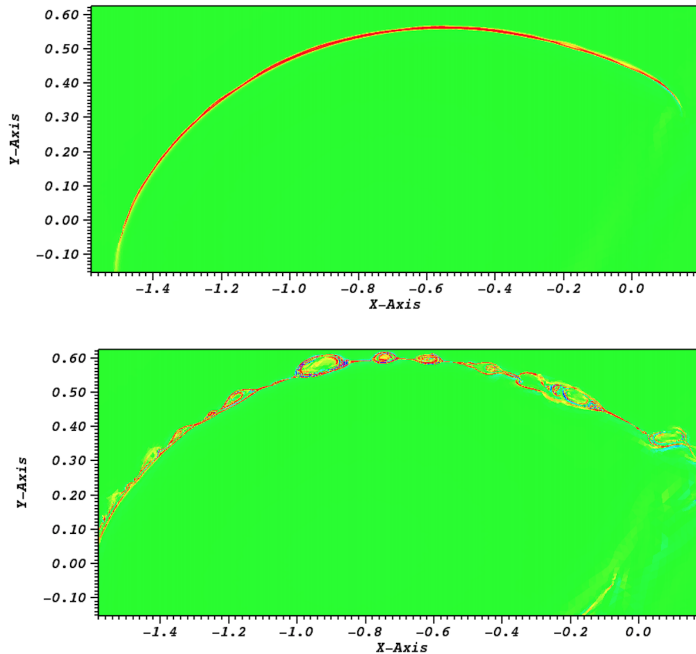


Figure 13. Same as previous figure for the case $S = 350000$, for the previous time spotted by the second asterisk in Figure 11 (upper panel), and for a slightly later time during the reconnection process (lower panel). Note that the integrity of the current layer is not lost for the upper plot.

instability leading to a current density increasing exponentially as $e^{2.6t}$. This triggering phase in our simulations has been carefully checked to agree with stability theory (Richard et al. 1990). As seen in Figure 6, the formation of the current sheets proceeds through a combination of thinning (as a is observed to decrease in time), stretching (as L is increasing), and a weak magnetic field strengthening, in agreement with the scenario suggested by Tolman et al. (2019).

We have defined two simple parameters characterizing the growth of the forming plasmoids. The first one, t_p , is the delay time between the birth of the first plasmoids (time at which they become to be barely visible in the current density structure) and the start of the formation of the current sheets (taken as the time at which the corresponding current density exceeds the equilibrium setup value). A rapidly converged constant value (with S) of $t_p = 2.4 \tau_A$ is obtained (see Figure 14). This delay time can be identified to correspond to the quiescent phase proposed in Comisso et al.’s scenario, during which many modes become progressively unstable and compete with each other (see Figures 3-4 in Comisso et al. (2017)). Indeed, the duration of this phase is predicted to be approximatively given by the time scale of the current sheet formation. This is also in agreement with a conclusion drawn in Uzdensky et al. (2016). A similar result has been obtained for the coalescence setup, with a slight difference for the highest S values where their time delay is non-monotonic and increases weakly again (Huang et al. 2017).

The second parameter, γ_p , is deduced from the second slope observed during the increase of the maximum current density (see Figure 11), and thus characterizes an abrupt growth phase following the slower previous quiescent phase. This explosive phase over a short time scale corresponds to the predicted phase dominated by the mode that emerges ”first” at the end of the linear phase in the theory of Comisso et al. Our results also qualitatively agree with the non-monotonic dependence with S , as a consequence of the non-power law dependence with S . Values $\gamma_p \tau_A \simeq 10$ are also obtained for the highest S values, thus confirming that $\gamma_p \tau_A \gg 1$ at the end of the linear phase. For $S \gtrsim S_c$, the scaling law given by SP stability theory with $\gamma_p \propto S^{1/4}$ is only marginally recovered. A very similar result has been obtained for the coalescence setup (Huang et al. 2017), except that $\gamma_p \tau_A \simeq 10 - 20$ are reported. The difference at relatively low S can be largely attributed to the reconnection outflow (neglected in theoretical models) that can affect the growth of the plasmoids and thus the scaling relations (Huang et al. 2019). As shown in previous studies, the noise induced by the numerical simulations also influences the results, and thus is an important parameter that needs to be investigated in future studies.

However, our results seem to contradict predictions from model of Pucci & Velli (2014), where the linear growth of plasmoids is constant and at most Alfvénic. This latter model is based on the existence of the critical aspect

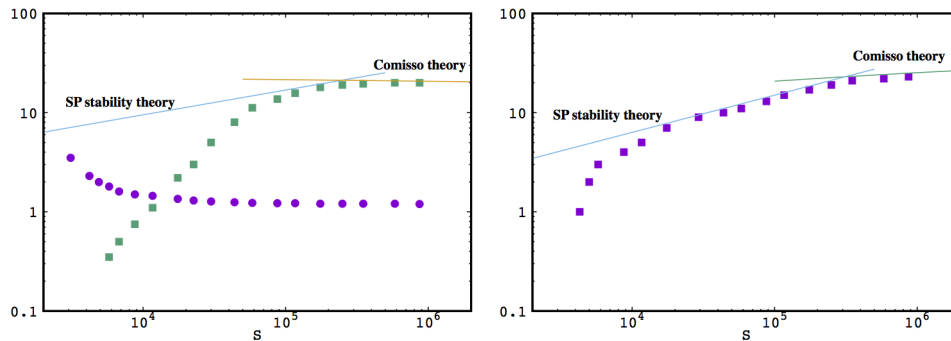


Figure 14. The two parameters characterizing the early growth of the plasmoids, t_p (in units of t_A , circles) and γ_p (in units of $1/t_A$, squares) as a function of S (left panel). The corresponding maximum number of plasmoids n_p (right panel), obtained at a time spotted by the third asterisk in previous figure. Theoretical power laws expected from SP linear theory scaling as $0.9 \times S^{1/4}$ and $0.2 \times S^{3/8}$, and asymptotic solutions from Equations (18-19) of (Comisso et al. 2016) are also plotted for comparison (see also text).

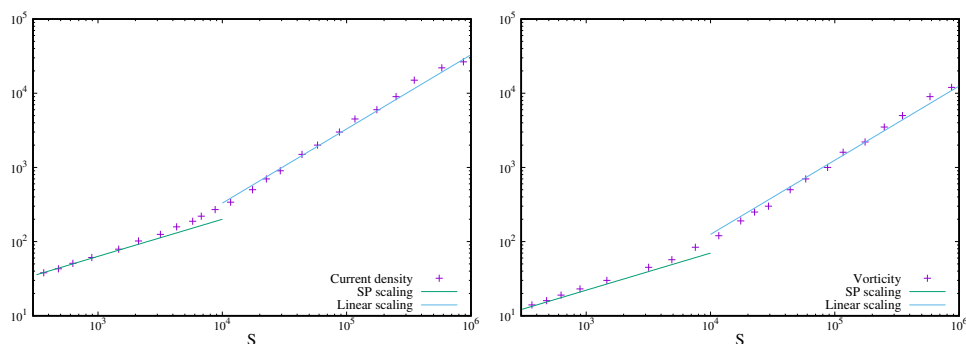


Figure 15. Overview of the maximum current density (left panel) and maximum vorticity (right panel) as a function of the Lundquist number S , for all the different runs. SP scaling laws in $2 \times S^{1/2}$ (for current density) and $0.75 \times S^{1/2}$ (for vorticity) are plotted, as well as linear scaling laws in $0.033 \times S$ (for current density) and $0.0125 \times S$ (for vorticity) approximating the plasmoid-dominated regime.

ratio $L/a \simeq S^{-1/3}$ for the disruption of the current sheet. We have measured the final aspect ratio just prior to the disruption in our runs, as plotted in Figure 16. Our results clearly show that the SP aspect ratio is reached only at low S , and final aspect ratio L/a turns to be bounded as $S^{1/3} < L/a < S^{1/2}$ at higher S . This is in agreement with the predicted bounding domain $\tau^{-2/3} S^{1/3} < L/a < S^{1/2}$ (Comisso et al. 2017).

Finally, our estimate of the time-averaged normalized reconnection rate is 0.014, that is two times higher than the value deduced from the coalescence setup. It is nevertheless in good agreement with values obtained in the literature of ~ 0.01 much higher than the Sweet-Parker rates, which could be sufficient to explain many disruptive events if the collisionnel regime apply. A fractal model (with hierarchical structure of the plasmoid chains that are effectively observed in simulations) based on heuristic arguments has been proposed to explain this fast rate independent of the Lundquist number (Huang & Bhattacharjee 2010). Indeed, to this end, a number of plasmoids (called non linear number) is required to scale linearly with S (Huang & Bhattacharjee 2010). Investigating this point is a complicated task requiring longer time simulations, and it will be the subject of a future study using tilt setup.

5. CONCLUSION

In this study we have demonstrated the usefulness to consider other configurations than the single Harris-type configuration or the coalescence instability to study the onset of the plasmoid-dominated reconnection regime in forming current sheets. Our results being very similar to the those obtained from the coalescence setup, suggest that Comisso et al.'s model is able to correctly predict the explosive growth of plasmoids leading to disruption of the reconnection current sheets when the initial configuration is ideally unstable. On the other hand, the other model developed by Pucci & Velli (2014) could apply when the initial configuration is ideally stable (and thus resistively unstable), as it has been validated using Harris-type current layer. This could explain the fastest time scale involved in the first category of setup compared to the second one.

The Lundquist number reached in this study is high enough in order match the relevant values for tokamaks. Indeed,

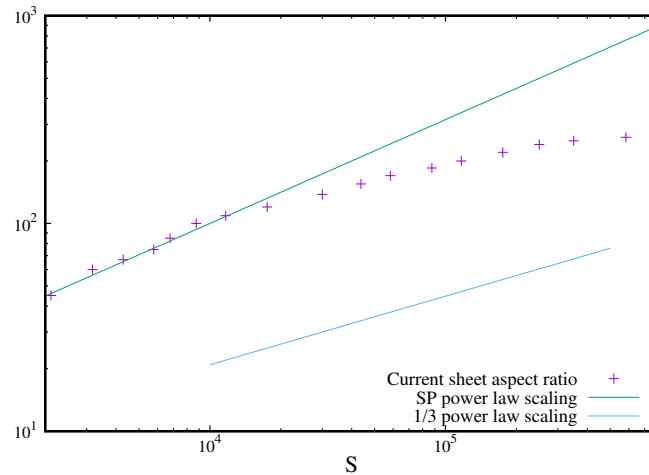


Figure 16. Current sheet aspect ratio values L/a , in SP reconnection regime for $S \lesssim 5 \times 10^3$, and just before disruption in plasmoid-dominated regime for higher S values. Theoretical power laws scaling as $S^{1/2}$ and $S^{1/3}$ are plotted for comparison.

the relevant S value for the internal disruption associated with the internal kink mode is $S \simeq 10^5$, as $S = 0.004S^*$ ($S^* = 2.5 \cdot 10^7$ being a standard Lundquist number value defined in terms of the toroidal magnetic field) (Günter et al. 2015). The corresponding width of the Sweet-Parker current layer is thus estimated to be $a \simeq 1$ cm, and the smallest length scale associated to the plasmoid structure is probably of order 1 mm or even smaller, reaching thus a scale close to the kinetic ones. Kinetic effects could be incorporated to our model in order to address this point. For example, the plasmoid instability has been shown to facilitate the transition to a Hall reconnection in Hall magnetohydrodynamical framework with an even faster reconnection rate of ~ 0.1 (Huang et al. 2011).

The smallest length scale associated to the plasmoid structure for $S = 10^6$ remains larger than the kinetic scale that is of order 10 m, when considering a solar loop structure and taking a length $L = 10^7$ m. However, as very high Lundquist number (at least 10^{10}) is required for the solar corona, kinetic effects could also play a role if the kinetic scale is reached via the plasmoid cascade at such huge Lundquist number.

REFERENCES

- BATY, H., & NISHIKAWA, H. 2016 Hyperbolic method for magnetic reconnection process in steady state magnetohydrodynamics. *MNRAS* **459** (1), 624–637, <https://doi.org/10.1093/mnras/stw654>
- BATY, H. 2019 FINMHD: An Adaptive Finite-element Code for Magnetic Reconnection and Formation of Plasmoid Chains in Magnetohydrodynamics. *The Astrophysical Journal Supplement Series* **243** (2), 23, <https://doi.org/10.3847/1538-4365/ab2cd2>
- BHATTACHARJEE, A., HUANG, Y.-M., YANG, H., & ROGERS, B. 2009 Fast reconnection in high-Lundquist-number plasmas due to the plasmoid instability. *Phys. Plasmas* **16** (11), 112102, <https://doi.org/10.1063/1.3264103>
- COMISSO, L., & GRASSO, D. 2016 Visco-resistive plasmoid instability. *Phys. Plasmas* **23** (3), 032111, <https://doi.org/10.1063/1.4942940>
- COMISSO, L., LINGAM, M., HUANG, Y. M., & BHATTACHARJEE, A. 2016 General theory of the plasmoid instability. *Phys. Plasmas* **23** (10), 100702, <https://doi.org/10.1063/1.4964481>
- COMISSO, L., LINGAM, M., HUANG, Y. M., & BHATTACHARJEE, A. 2017 Plasmoid instability in forming current sheets. *The Astrophysical Journal* **850**, 142, <https://doi.org/10.3847/1538-4357/aa9789>
- GÜNTER, S., YU, Q., LACKNER, K., BHATTACHARJEE, A., & HUANG, Y. M. 2015 Fast sawtooth reconnection at realistic Lundquist numbers. *Plasma Phys. Control. Fusion* **57** (1), 014017, <https://doi.org/10.1088/0741-3335/57/1/014017>
- HECHT, F. 2012 New development in FreeFem++. *Journal of Numerical Mathematics* **20**, 251–266, <https://doi.org/10.1515/jnum-2012-0013>
- HUANG, Y. M., COMISSO, L., & BHATTACHARJEE, A. 2017 Plasmoid instability in evolving current sheets and onset of fast reconnection. *The Astrophysical Journal* **849** (2), 75, <https://doi.org/10.3847/1538-4357/aa906d>
- HUANG, Y. M., & BHATTACHARJEE, A. 2010 Scaling laws of resistive magnetohydrodynamic reconnection in the high-Lundquist-number, plasmoid-unstable regime. *Phys. Plasmas* **17**, 062104, <https://doi.org/10.1063/1.3420208>
- HUANG, Y. M., BHATTACHARJEE, A., & SULLIVAN, B. P. A. 2011 Onset of fast reconnection in Hall magnetohydrodynamics mediated by the plasmoid instability. *Phys. Plasmas* **18**, 072109, <https://doi.org/10.1063/1.3606363>
- HUANG, Y. M., COMISSO, L., & BHATTACHARJEE, A. 2019 Scalings pertaining to current sheet disruption mediated by the plasmoid instability. *Phys. Plasmas* **26** (9), 092112, <https://doi.org/10.1063/1.5110332>
- KEPPENS, R., PORTH, O., GALSGAARD, K., ET AL. 2013 Resistive magnetohydrodynamic reconnection: Resolving long-term, chaotic dynamics. *Phys. Plasmas* **20** (9), 092109, <https://doi.org/10.1063/1.4820946>
- KEPPENS, R., PORTH, O., & XIA, C. 2014 Interacting tilt and kink instabilities in current channels. *The Astrophysical Journal* **795**, 77, <https://doi.org/10.1088/0004-637X/795/1/77>

- KNOLL, D. A., & CHACÓN, L. 2006 Coalescence of magnetic islands, sloshing, and the pressure problem. *Phys. Plasmas* **13** (3), 032307, <https://doi.org/10.1063/1.2173515>
- LANKALAPALLI, S., FLAHERTY, J. E., SHEPHARD, M. S., & STRAUSS, H. R. 2007 An adaptive finite element method for magnetohydrodynamics. *Journal of Computational Physics* **225** (1), 363-381, <https://doi.org/10.1006/jcph.1998.6091>
- LOUREIRO, N. F., SCHEKOCIHIN, A. A., & COWLEY, S. C. 2007 Instability of current sheets and formation of plasmoid chains. *Phys. Plasmas* **14** (10), 100703, <https://doi.org/10.1063/1.2783986>
- LOUREIRO, N. F., SAMTANEY, R., & UZDENSKY, D. A. 2012 Magnetic reconnection and stochastic plasmoid chains in high-Lundquist-number plasmas. *Phys. Plasmas* **19** (4), 042303, <https://doi.org/10.1063/1.3703318>
- NG, C. W., ROSENBERG, D., GERMASCHEWSKI, K., POUQUET, A., & BHATTACHARJEE, A. 2007 A comparison of spectral element and finite difference methods using statically refined nonconforming grids for the MHD island coalescence instability problem. *The Astrophysical Journal Supplement Series* **177** (2), 613-625, <https://doi.org/10.1086/588139>
- SAMTANEY, R., LOUREIRO, N. F., UZDENSKY, D. A., SCHEKOCIHIN, A. A., & COWLEY, S. C. 2009 Formation of plasmoid chains in magnetic reconnection. *Phys. Rev. Lett.* **103** (10), 105004, <https://doi.org/10.1103/PhysRevLett.103.105004>
- SWEET, P. A. 1958 The neutral point theory of solar flares. In *Electromagnetic Phenomena in Cosmical Physics* (ed. Lehnert B). p. 123. Cambridge: Cambridge University Press.
- PARK, MONTICELLO, D. A., AND WHITE, R. B. 1984 Reconnection rates of magnetic fields including the effects of viscosity. *Phys. Fluids* **27**, 137, <https://doi.org/10.1063/1.864502>
- PARKER, E. N. 1957 Sweet's mechanism for merging magnetic fields in conducting fluids. *J. Geoph. Research.* **62**, 50520, <https://doi.org/10.1029/JZ062i004p00509>
- PHILIP, B., PERNICE, M., & CHACON, L. 2007 Solution of reduced resistive magnetohydrodynamics using implicit adaptive mesh refinement. *Lecture Notes in Computational Science and Engineering* **55**, 723-729, https://doi.org/10.1007/978-3-540-34469-8_90
- PRIEST, E. R., & FORBES, T. G. 2000 Magnetic Reconnection. (Cambridge: Cambridge Univ. Press), <https://doi.org/10.1017/CBO9780511525087>
- PUCCI, F., & VELLI, M. 2014 Reconnection of quasi-singular current sheets: the 'ideal' tearing mode. *The Astrophysical Journal Letters* **780** (2), L19, <https://doi.org/10.1088/2041-8205/780/2/L19>
- PUCCI, F., VELLI, M., TENERANI, A., & DEL SARTO, D. 2018 Onset of fast ideal tearing in thin current sheets: Dependence on the equilibrium current profile. *Phys. Plasmas* **25** (3), 032113, <https://doi.org/10.1063/1.5022988>
- RICHARD, R. L., SYDORA, R. D., & ASHOUR-ABDALLA, M. 1990 Magnetic reconnection driven by current repulsion. *Phys. Fluids B* **2**, 488-494, <https://doi.org/10.1063/1.859338>
- RIPPERDA, B., PORTH, O., XIA, C., & KEPPENS, R. 2017 Reconnection and particle acceleration in interacting flux ropes I. Magnetohydrodynamics and test particles in 2.5D. *MNRAS* **467**, 3279-3298, <https://doi.org/10.1093/mnras/stx379>
- STRAUSS, H. R., & LONGCOPE, D. W. 1998 An Adaptive Finite Element Method for Magnetohydrodynamics. *Journal of Computational Physics* **147** 318, <https://doi.org/10.1006/jcph.1998.6091>
- TENERANI, A., VELLI, M., RAPAZZO, A. F., & PUCCI, F. 2015 Magnetic reconnection: recursive current sheet collapse triggered by 'ideal' tearing. *The Astrophysical Journal Letters* **813**, L32, <https://doi.org/10.1088/2041-8205/813/2/L32>
- TENERANI, A., VELLI, M., PUCCI, F. LANDI, S., M., AND RAPAZZO, A. F. 2016 'Ideally' unstable current sheets and the triggering of fast magnetic reconnection. *Journal of Plasma Physics* **82** (5), 535820501, <https://doi.org/10.1017/S002237781600088X>
- UZDENSKY, D. A., LOUREIRO, & N. F., SCHEKOCIHIN, A. A. 2010 Fast magnetic reconnection in the plasmoid-dominated regime. *Phys. Rev. Lett.* **105** (23), 235002, <https://doi.org/10.1103/PhysRevLett.105.235002>
- UZDENSKY, D. A., LOUREIRO, & N. F., SCHEKOCIHIN, A. A. 2010 Magnetic reconnection onset via disruption of a forming current sheet by the tearing instability. *Phys. Rev. Lett.* **116** (10), 105003, <https://doi.org/10.1103/PhysRevLett.116.105003>